JYX JYVÄSKYLÄN YLIOPISTO UNIVERSITY OF JYVÄSKYLÄ

This is a self-archived version of an original article. This version may differ from the original in pagination and typographic details.

Author(s): Mentel, Kamila K.; Emelianov, Aleksei V.; Philip, Anish; Johansson, Andreas; Karppinen, Maarit; Pettersson, Mika

Title: Area-Selective Atomic Layer Deposition on Functionalized Graphene Prepared by Reversible Laser Oxidation

Year: 2022

Version: Published version

Copyright: © 2022 The Authors. Advanced Materials Interfaces published by Wiley-VCH Gmb

Rights: CC BY-NC 4.0

Rights url: https://creativecommons.org/licenses/by-nc/4.0/

Please cite the original version:

Mentel, K. K., Emelianov, A. V., Philip, A., Johansson, A., Karppinen, M., & Pettersson, M. (2022). Area-Selective Atomic Layer Deposition on Functionalized Graphene Prepared by Reversible Laser Oxidation. Advanced Materials Interfaces, 9(29), Article 2201110. https://doi.org/10.1002/admi.202201110

ADVANCED MATERIALS INTERFACES
www.advmatinterfaces.de

Area-Selective Atomic Layer Deposition on Functionalized Graphene Prepared by Reversible Laser Oxidation

Kamila K. Mentel, Aleksei V. Emelianov, Anish Philip, Andreas Johansson, Maarit Karppinen, and Mika Pettersson**

Area-selective atomic layer deposition (ALD) is a promising "bottom-up" alternative to current nanopatterning techniques. While it has been successfully implemented in traditional microelectronic processes, selective nucleation of ALD on 2D materials has so far remained an unsolved challenge. In this article, a precise control of the selective deposition of ZnO on graphene at low temperatures (<250 °C) is demonstrated. Maskless femtosecond laser writing is used to locally activate predefined surface areas (down to 300 nm) by functionalizing graphene to achieve excellent ALD selectivity (up to 100%) in these regions for 6-nm-thick ZnO films. The intrinsic conductive properties of graphene can be restored by thermal annealing at low temperature (300 °C) without destroying the deposited ZnO patterns. As the graphene layer can be transferred onto other material surfaces, the present patterning technique opens new attractive ways for various applications in which the functionalized graphene is utilized as a template layer for selective deposition of desired materials.

1. Introduction

Atomic layer deposition (ALD) is one of the cornerstones of the semiconductor industry.[1] In ALD, the film growth relies on self-limiting gas-surface reactions of two different precursors sequentially pulsed into the reactor, and yields—as the benchmark of the technique—highly conformal, large-area homogeneous, and pinhole-free coatings with precise thickness control. However, under certain conditions, this fundamental scheme can be intentionally broken such that the film growth can be selectively limited to predetermined surface areas only. Currently, this area-selective ALD (AS-ALD) approach is attracting increasing interest, as it has the capacity to address the long-term dream of bottom-up fabrication of the active material components.[2–5] Compared with the conventional top-down photolithography technology, consisting of multiple demanding processing steps, bottom-up patterning is much simpler in principle. Moreover, it helps to minimize pattern placement errors, which have become increasingly important as device dimensions continue to shrink.

Unfortunately, targeted lateral control of the film growth contradicts the fundamental principle of ALD. To address this contradiction, surface chemistries are spatially manipulated in AS-ALD to create local differences, so that the film growth can be limited to the desired areas only; this has been attempted by a variety of different approaches.[6–11] The degree of selectivity, defined by the difference in the growth rates on the fast-growth and limited-growth areas, can be considered the most crucial criterion for an AS-ALD process. The next items on the wish-list would be flexibility regarding the pattern design (shapes, sizes, frequencies, etc.) and versatility regarding the variety of compatible ALD processes.

A majority of the AS-ALD processes are based on the deactivation of certain areas on the substrate, using, e.g., small-molecule inhibitors, plasma treatments, ion implantation, or—most commonly—so-called self-assembled monolayers (SAMs) of linear organic molecules with appropriate tail groups.[4] In practice, there are numerous issues related to these approaches, such as the loss of selectivity during the film deposition and the fact that such techniques are limited to ultrathin films. Moreover, most of the deactivation-based AS-ALD approaches require multiple processing steps. A significantly simpler approach regarding the required processing steps would be to rely on local activation instead of local deactivation.[4] A prime example is the use of catalytic seed layers to accelerate the film

K. K. Mentel, A. V. Emelianov, A. Johansson, M. Pettersson
Department of Chemistry
Nanoscience Center
University of Jyväskylä
Jyväskylä FI-40014, Finland
E-mail: mika.j.pettersson@jyu.fi

A. Philip, M. Karppinen
Department of Chemistry and Materials Science
School of Chemical Engineering
Aalto University
Aalto, Espoo FI-00076, Finland
E-mail: maarit.karppinen@aalto.fi

A. Johansson
Department of Physics
Nanoscience Center
University of Jyväskylä
Jyväskylä FI-40014, Finland

The ORCID identification number(s) for the author(s) of this article can be found under https://doi.org/10.1002/admi.202201110.

© 2022 The Authors. Advanced Materials Interfaces published by Wiley-VCH GmbH. This is an open access article under the terms of the Creative Commons Attribution-NonCommercial License, which permits use, distribution and reproduction in any medium, provided the original work is properly cited and is not used for commercial purposes.

DOI: 10.1002/admi.202201110

growth on the selected areas.[12] However, these approaches typically suffer from lower selectivity.

Metal oxide films are key active materials in various applications. Notably, the metal oxide/carbon surface junction has attracted increasing attention as a promising platform for photodetectors,[13] gas-sensors,[14] electrodes for supercapacitors,[15] and photocatalysts,[16] and using graphene as the carbon source is of interest in particular thanks to its extraordinary properties.[17,18] Nonetheless, the use of pristine graphene for the ALD is quite challenging, as its sp^2-hybridized carbon atoms are intrinsically free of the reactive surface sites required for the ALD nucleation. Different procedures have been used to overcome the inertness of graphene toward ALD precursors, such as chemical pretreatment,[19] noncovalent functionalization with organic molecules,[20,21] or plasma exposure prior to or during the ALD.[22]

A promising approach for increasing surface reactivity of graphene is its functionalization with oxygen species. Theoretical calculations have predicted that among the different chemical species used to functionalize carbon nanomaterials, carboxyl (−COOH) and carbonyl groups (−C=O) are key nucleation centers that improve the ALD process of ZnO at low temperatures.[23] In addition, species containing −OH groups cause the formation of metal-oxide supports in graphite and graphene, as they function as proton exchangers with the metal precursor ligands. Furthermore, the chemical activity and selectivity of different functional groups contribute to obtaining a precise thickness control and high uniformity; thus, the density of active sites plays an important role.[24]

Previously, our group has demonstrated a femtosecond laser irradiation technique based on a two-photon oxidation (2-PO) process, wherein oxygen containing groups are incorporated into the graphene lattice through exposure to femtosecond laser pulses under ambient atmosphere.[25–27] This leads to the formation of hydroxyl and epoxy groups on the graphene surface under moderate laser exposures and carboxyl groups at near-to-ablation exposure levels.[28] This technique allows for tuning the oxidation level of the graphene[28] and for the possibility of preparing arbitrary patterns with high spatial resolution (300 nm). Additionally, all-optical patterning is a simple and chemical-free direct write method.

In this article, we present the proof-of-concept for the AS-ALD on monolayer graphene consisting of three steps: (i) area-activation via two-photon oxidation, (ii) ALD, and (iii) thermal annealing, schematically represented in **Figure 1**. The laser-induced functional groups in graphene acted as the active sites that facilitate the nucleation of the precursors during the ALD step, while pristine graphene served as an ideal nongrowth surface for locally deactivated AS-ALD. Hence, the oxidized patterns exhibited superior selectivity to ALD with respect to pristine graphene. We chose the diethyl zinc (DEZ) plus water process for our proof-of-concept experiments, not only because it is one of the original prototype ALD processes but also because ZnO, as a wide and direct bandgap semiconductor, has tunable optical and electronic properties that are attractive for various applications.[29] Thin ZnO layers (<7 nm) were selectively deposited on oxidized patterns on graphene with a tested range of defect (active site) density, n_D, from 1.4×10^{11} up to 7.5×10^{11} cm^{-2}. Thus, the metal oxide could be deposited on graphene with properties tuned from conductive to nearly insulating.[25,30] Higher laser irradiation doses led to a more uniform, smoother layer deposition due to a higher density of active sites. Moreover, we show that graphene properties could be restored after ALD treatment using thermal annealing, without altering the deposited metal oxide layer. A recovery of graphene properties is important for metal oxide/graphene composite device integration, providing improved optical and electronic properties.

2. Results and Discussion

We fabricated 5×5 mm^2 Si chips with a 295-nm-thick SiO_2 layer, deposited Pd grids, and transferred a graphene layer onto the top via a polymethyl methacrylate (PMMA)-assisted method (see Experimental section). A chosen area of 30×25 μm^2 was cleaned of the residual PMMA and amorphous carbon with an atomic force microscope (AFM) tip in contact mode prior to the two-photon oxidation, as these residues could act as undesired nucleation sites for ALD on pristine graphene.[31] To activate the chosen areas for the selective ALD, we used 2-PO induced by femtosecond laser exposure in ambient atmosphere. For that, a

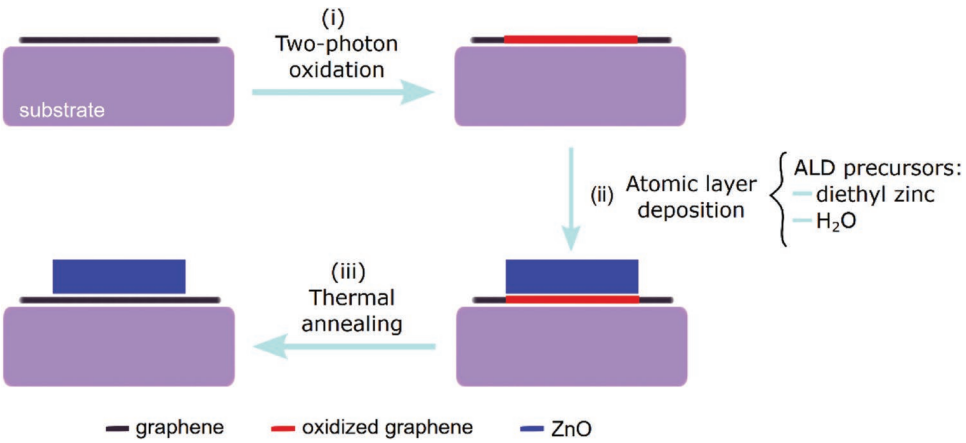

Figure 1. Scheme of AS-ALD on monolayer graphene. i) Area-activation via two-photon oxidation, ii) atomic layer deposition of ZnO, and iii) thermal annealing.

© 2022 The Authors. Advanced Materials Interfaces published by Wiley-VCH GmbH

matrix of nine-oxidized squares (2×2 μm^2 each) was prepared with photon doses from 90 up to 625 pJ^2 s, where the dose is described as the squared pulse energy multiplied by an exposure time per spot. The thus-patterned sample was exposed to 63 ALD (DEZ+H_2O) cycles at 200 °C, followed by thermal annealing at 300 °C for 2 h in an argon atmosphere.

Figure 2a–c shows optical images of the sample taken after each sample preparation step, i.e., 2-PO, ALD, and thermal annealing. The first striking observation was that the oxidized patterns, which were originally not visible under an optical microscope, became easily distinguishable from the pristine graphene after ALD, and remained visible after thermal annealing. The emerging contrast between the patterned and pristine areas indicates the increased height of the patterned regions.

To ensure that this difference was caused by the 2-PO technique, detailed AFM measurements were performed to follow the surface modifications introduced by each step of sample preparation. Figure 2d shows the topography image of patterns prepared with 2-PO. The oxidized patterns were slightly elevated (≈2 nm) compared with pristine graphene. It was reported previously that the island-like structures observed in regions exposed to very low optical doses merged into a smooth, slightly elevated layer in moderately oxidized graphene.[26] Figure 2e shows the AFM topography image for the same sample after the 63 ALD cycles. It was apparent that the ZnO deposition selectively covered only the oxidized patterns, producing metal oxide film on top of the oxidized areas that were a few nanometer thick. This was due to the fact that the oxygen groups incorporated with 2-PO reacted with the DEZ precursor, thus allowing its nucleation. For ALD at 200 °C, no deposition of ZnO was seen on pristine graphene, which was not exposed to femtosecond laser pulses (Figure S1, Supporting

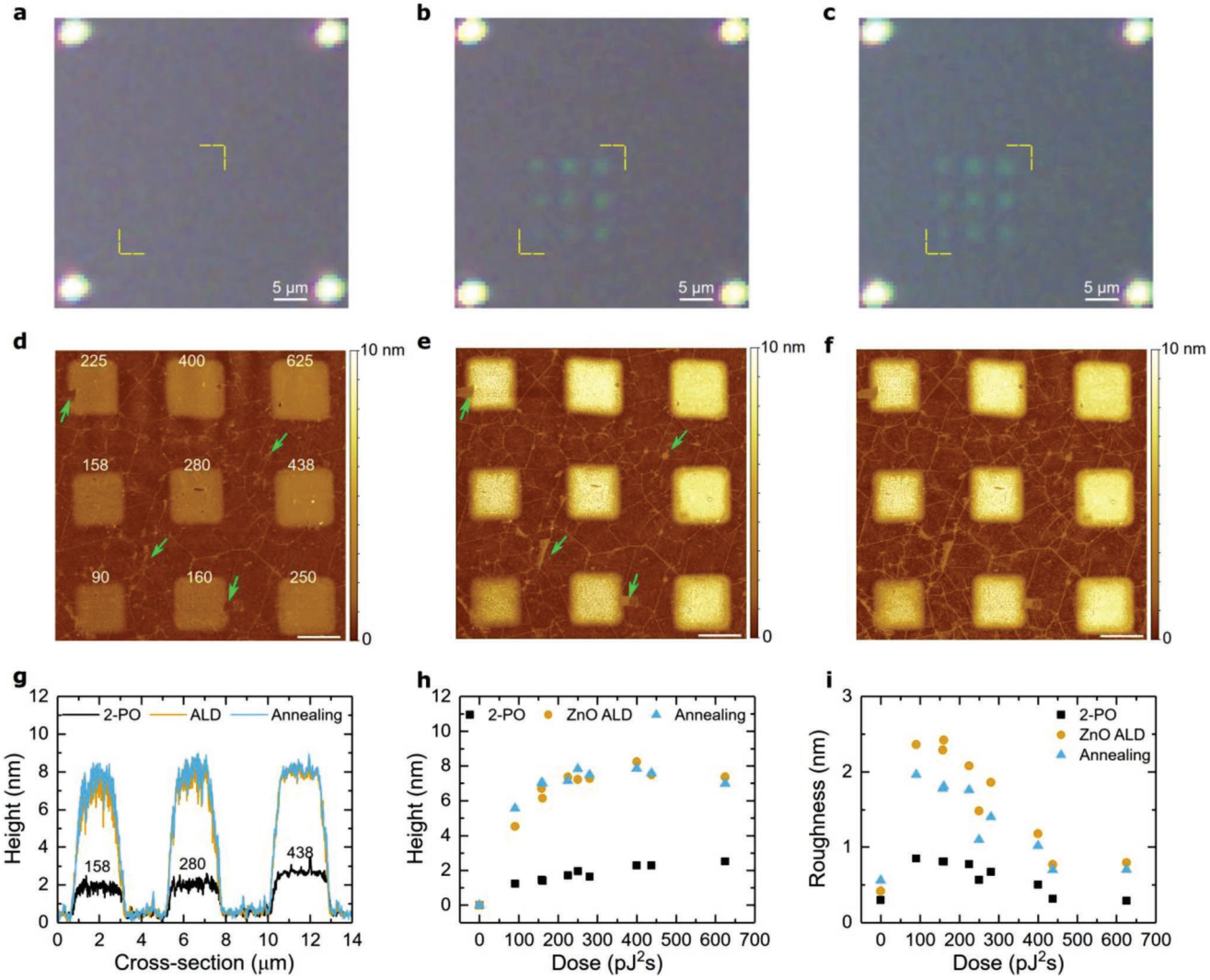

Figure 2. Area-selective ALD on graphene template. a–c) Optical microscope and d–f) AFM topography images after each step of sample preparation: a,d) two-photon oxidation, b,e) 63 cycles of ALD at 200 °C, and c,f) thermal annealing for 2 h at 300 °C in Ar atmosphere. The laser doses (pJ^2 s) used for oxidizing the squares are marked on top of the squares in (d). Few examples of tiny SiO_2 regions exposed due to rupture of graphene layer during AFM contact mode cleaning are indicated with the green arrows (d) before and (e) after ALD. Scale bars on AFM images are 2 μm. g) Narrow cross-sections (averaged across 200 nm) drawn through the middle of the patterns created with laser doses of 158, 280, and 438 pJ^2 s. h) Height and i) root-mean-square roughness as a function of dose, extracted for each step of sample preparation.

 © 2022 The Authors. Advanced Materials Interfaces published by Wiley-VCH GmbH

Information). The chosen ALD experimental parameters also reduced the deposition on the wrinkles outside of the patterned region, due to reduced physisorption of the precursor. The growth on folds is lesser than on the laser-activated areas. The minor deposition is related to the remaining impurities, which are trapped on the folds during the contact mode cleaning. An additional contact mode cleaning by scanning at different direction should further improve cleanness of the sample. A small degree of deposition was visible on the substrate (SiO_2) that was exposed due to damage to the graphene film during contact mode cleaning. Four such areas are marked by green arrows in Figure 2d,e. To avoid damage of the graphene film, the smaller forces need to be used while scanning in contact mode. There was no visible topography change after thermal annealing (Figure 2f).

The quality and cleanliness of graphene are crucial for selective deposition over the target area. The selectivity may be hindered by the presence of impurities on the sample surface that can provide additional nucleation sites. Loss of selectivity due to surface contamination by polymer residues was found to be more pronounced for the ALD deposition performed at a lower temperature (Figures S1 and S2, Supporting Information). This brings attention to the importance of ultraclean graphene preparation. Even commonly established synthesis and transfer methods leave contamination on the surface of the graphene,[32] which affects not only its properties but also the postdeposition treatment steps.

In Figure 2g, narrow cross-section of patterns prepared with photon doses of 158, 280, and 438 pJ^2 s are compared. Most remarkably, ZnO was deposited only epitaxially, without any expansion of the patterns in lateral direction. The lack of lateral growth is of immense importance for the precise device fabrication (e.g., no misalignment problem). Patterns prepared with higher doses presented more uniform deposition. The average heights of patterns created with 2-PO and subsequent ALD and thermal annealing steps, extracted from the AFM height images, are presented as a function of dose in Figure 2h; to obtain the thickness of the deposited ZnO, the pattern height after the 2-PO needs to be subtracted from the total height. The data show that the thinnest ZnO deposition (3.3 nm) occurred for the area prepared with the lowest laser photon dose (90 pJ^2 s). The thickness increased with increasing dose, until it reached a plateau at 6 nm for the pattern prepared with 225 pJ^2 s. As the ZnO depositions were carried out with 63 ALD cycles, the maximum ZnO deposition height of ≈6 nm translates into the growth-per-cycle (*GPC*) value of ≈1 Å for the patterned regions, while the growth was completely suppressed for the pristine graphene areas. This *GPC* value on the patterned regions was smaller than the growth on the reference silicon wafer (a *GPC* ≈ 1.6 Å; measured with XRR). For the ZnO ALD process, it is well known that the *GPC* decreases with increasing deposition temperature,[33] and this was also seen for our tests with higher temperature depositions on patterned graphene (Note S2 and Figure S2, Supporting Information).

Figure 2i shows the extracted root-mean-square (*RMS*) roughness as a function of laser dose. Pristine graphene had a roughness of 0.3 nm. The 2-PO patterns prepared with low laser doses exhibited higher roughness (*RMS* = 0.85 nm for 90 pJ^2 s) consistent with the formation of island-like structures through the incorporation of oxygen-containing groups. For higher doses, the islands merged and consequently the sample roughness decreased (*RMS* = 0.29 nm for dose 625 pJ^2 s). A substantial increase in roughness was observed for all patterns after the ALD; however, a higher degree of roughness was found in the patterns prepared with low doses. Increased roughness was caused by the nucleation at the functional groups. We can infer that ZnO deposition followed a Volmer–Weber (island) growth mode, with nucleation following the functional group distribution. Deposited ZnO clustered in the form of pillars for low laser dose (*RMS* = 2.36 nm for dose 90 pJ^2 s) and coalesced to a more uniform layer for patterns prepared with higher doses (*RMS* ≈ 0.8 nm for doses ≥438 pJ^2 s) that contained more densely packed functional groups. Hence, the use of higher doses was beneficial for achieving a uniform, pinhole-free thin layer of ALD material. The same growth mode was reported for the deposition of ZnO on graphene/SiO_2 and graphene oxide/SiO_2 using thermal evaporation of metallic Zn under an oxygen atmosphere at room temperature.[34] The roughness decreased slightly after thermal annealing. This could have been due to improved ZnO crystallinity.

Raman spectroscopy was used to assess the effect of each step of sample preparation on the properties of the graphene through investigation of the various characteristic peaks and relations between them. The G band (≈1580 cm^{-1}) is common to all graphitic materials, and it corresponds to the in-plane sp^2 C—C stretching mode. The 2D band (≈2685 cm^{-1}) originates from the in-plane breathing-like mode of the carbon ring. The G and 2D band positions shift due to stress or doping of the graphene.[35] Additionally, the disorder-induced D (≈1350 cm^{-1}) and D' (≈1620 cm^{-1}) bands are activated in the presence of defects (e.g., sp^3-type defects). The area of the D band/area of the G band (A_D/A_G) is a good measure of defect concentration.[36] It is found to increase for higher photons/ions exposures,[27,28,36] indicating a change of crystalline graphene into a nanocrystalline phase (stage 1).[35] Further increase to the exposure causes higher lattice disorder (stage 2),[35] observed as a decrease of A_D/A_G with simultaneous broadening of the G band.[27,28,36]

The creation of active sites to facilitate the nucleation is necessary to perform ALD on a graphene surface. It has been shown that laser-induced 2-PO breaks the sp^2-bonds in graphene and forms sp^3-type defects with out-of-plane covalent functional groups.[28] The level of defect formation is controlled by irradiation dose, which then is reflected in the strength of the D band in Raman spectra. The effect of laser irradiation is illustrated in **Figure 3**a, by plotting the Raman spectra (λ_{Laser} = 532 nm) collected from the pristine graphene region and at the center of the patterns prepared with doses of 158, 280, and 438 pJ^2 s. Pristine graphene exhibited good quality prior to any treatment, with a negligible D band ($n_D \approx 3.3 \times 10^{10}$ cm^{-2}). The small but broad signal at ≈1200–1600 cm^{-1} was assigned to the carbonized form of PMMA, which remained on graphene surface from the sample preparation step.[32] Interestingly, it could be partially removed with laser exposure (Figure S3, Supporting Information). After 2-PO, the D band at 1345 cm^{-1} and the D' band at ≈1620 cm^{-1} were clearly visible. Increasing the laser dose increased the intensity of these bands, while the 2D band became weaker, showing an increase of defect concentration and higher lattice disorder. Patterns prepared with doses of

© 2022 The Authors. Advanced Materials Interfaces published by Wiley-VCH GmbH

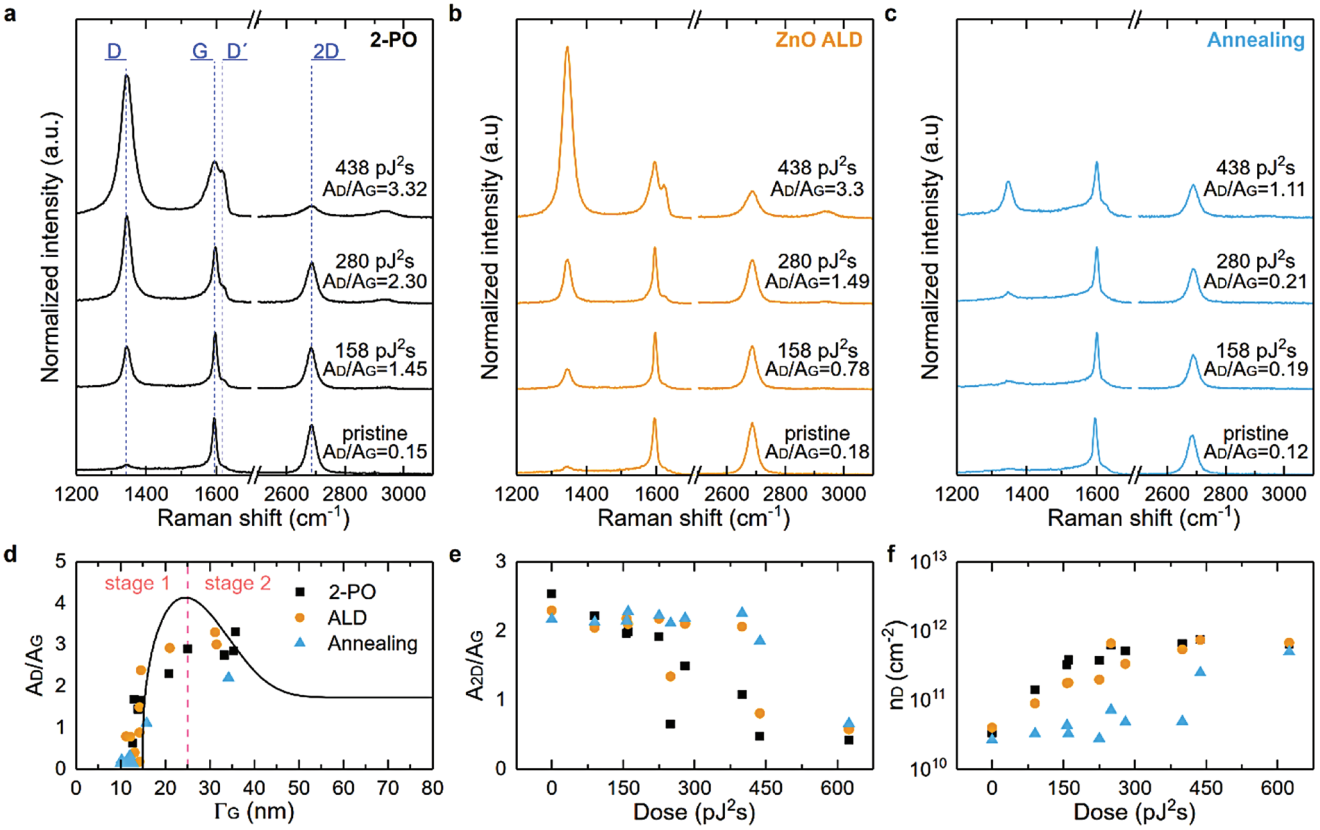

Figure 3. Raman spectroscopy analyses. The Raman spectra collected from graphene chip after each step of sample preparation: a) two-photon oxidation, b) 63 cycles of ALD at 200 °C, and c) thermal annealing at 300 °C for 2 h in Ar atmosphere. Spectra were collected at the center of the squares produced with indicated doses and in the pristine region. Spectra were background-corrected and normalized in relation to the G band. Spectra were offset for clarity. The A_D/A_G ratio is marked next to each spectrum. d) A_D/A_G as a function of the full width at half maximum of the G band, Γ_G. The solid line represents point defect (see Cançado et al.[36] for more details). e) A_{2D}/A_G and f) defect density, n_D, as a function of dose. Legend the same as in (d). The extracted data were obtained by fitting the Raman spectra with Lorentzian curves to the D, G, and 2D bands.

158, 280, and 438 pJ^2 s had, respectively, A_D/A_G ratios of 1.45, 2.30, and 3.32, and a defect density of 3.3×10^{11}, 5.2×10^{11}, and 7.5×10^{11} cm^{-2}. The defect sites are mainly hydroxyl and epoxy groups for moderate laser doses, and carboxyl groups at near-to-ablation exposures.[28] The hydroxyl and carboxyl groups are good nucleation centers for ALD, and therefore can act as an active template for the subsequent ZnO growth.

After ALD, the D and D' bands decreased and the 2D band increased in intensity (Figure 3b), which was interpreted to originate from the partial removal of defects. These observations show that the ALD step did not deteriorate the quality of graphene. On the contrary, it somewhat improved graphene properties. This could be related to the dissociation of the functional groups during the purging step or due to ALD being performed at elevated temperature (200 °C), leading to simultaneous healing of defects. Furthermore, we did not observe a significant shift of the G and 2D bands, which would have indicated a strong interaction of graphene with the deposited ZnO films (e.g., charge density modulation or mechanical strain). We did not observe Raman peaks characteristic for ZnO in the spectra using 532 nm laser. This is probably due to the ZnO layers being too thin, which results in a signal that is too weak to be detected.

When the sample was thermally annealed after the ALD step (at 300 °C for 2 h in Ar atmosphere), a clear decrease of the D and D' bands and an even further increase of the 2D band were observed (Figure 3c). This important finding showed that graphene transformed from the oxidized form to pristine form. Additionally, a small blue shift of the G band (up to 6 cm^{-1}) and the 2D band (up to 5 cm^{-1}) was observed, which could be triggered by the weak compressive stress of recrystallized thin film on the graphene underneath[37,38] or doping induced by carbonization of PMMA residues.

Figure 3d presents A_D/A_G ratio as a function of the full width at half maximum (Γ_G) of the G band for all patterns and for the pristine region. The applied laser doses created patterns in both disorder stages: stage 1 (low dose) and stage 2 (moderate dose). After the ALD, a small decrease of A_D/A_G and narrowing of Γ_G was observed. Thermal annealing further reduced A_D/A_G with simultaneous narrowing of the G band, indicating the removal of laser-induced sp^3-type defects and an improved crystalline graphene lattice, i.e., the healing of graphene.

The ratio (A_{2D}/A_G), shown in Figure 3e, provides information about the crystallinity of graphene. The highest ratio was found in the pristine graphene (2.53), and after 2-PO the A_{2D}/A_G decreased, with the lowest A_{2D}/A_G (0.42) taken from the pattern prepared with 625 pJ^2 s dose. The ALD (for low doses) and thermal annealing (except the highest dose) led to an increase of A_{2D}/A_G, bringing it close to the value of the

© 2022 The Authors. Advanced Materials Interfaces published by Wiley-VCH GmbH

pristine graphene showing that the crystallinity of graphene was restored.

Figure 3f shows the defect density as a function of laser dose, extracted from the A_D/A_G ratio.[36] Upon irradiation, n_D increased up to 23 times compared with pristine graphene (3.3×10^{10} cm^{-2}). Even the lowest dose (90 pJ^2 s, $n_D = 1.4\times10^{11}$ cm^{-2}, A_D/A_G = 0.63) led to the deposition of a dense but not fully uniform ZnO layer. It showed that low level oxidation could improve nucleation, while underlaying graphene retains rather unaffected properties close to pristine graphene. Higher defect concentrations (more densely packed groups) led to more uniform ZnO film (smaller roughness). The following ALD step only slightly lowered the defect concentration. Therefore, a layer of a few-nanometer-thick metal oxide on top of graphene with different conductive properties is feasible via controllable defect engineering. On the other hand, thermal annealing considerably reduced the defect concentration down to 3–5 × 10^{10} cm^{-2}, which was very close to the defect density of pristine graphene. Thus, 2 h of thermal annealing at 300 °C under argon atmosphere was sufficient to almost recover the graphene properties as they were before 2-PO functionalization. Longer annealing time would presumably lead to the full recovery of the graphene layer. It is worth mentioning that thermal annealing is commonly used for defect healing of defects introduced into the graphene lattice. However, typically the process requires a highly elevated temperature (e.g., 1000 °C, in vacuum)[39] for full graphene recovery, while in our approach 300 °C was sufficient to repair the graphene lattice. Lower healing temperatures were also reported for graphene samples where defects were created by aluminum oxide plasma.[38] It seems that attached metal oxides may facilitate healing process in graphene. Our finding shows that graphene properties can be regained after completing the AS-ALD process, which is important for electronic device applications. For example, it was shown that a ZnO/graphene composite thin-film transistor exhibits higher conductivity with enhanced carrier mobility when compared with a ZnO thin-film transistor.[40]

We used energy-dispersive X-ray spectroscopy (EDS) to confirm the presence of ZnO on the surface of the sample. The spectral contribution of detected elements is presented in Figure S4 (Supporting Information). The carbon (K_α = 0.28 eV), oxygen (K_α = 0.53 eV), and silicon (K_α = 1.74 eV) transitions were found on the pristine and patterned region. Additionally, a weak Zn signal (L_α = 1.12 eV) was detected on the patterned squares. No Zn signal was detected on pristine graphene. Even though EDS is not very sensitive to signals from thin layers, the lack of the Zn peak in the EDS spectrum in the pristine region together with the AFM images analysis allows us to conclude that pristine graphene was free of metal oxide. In Figure S4 (Supporting Information), we show the dependence of the Zn wt% deposited onto the graphene surface versus the irradiation dose of the fs laser. The trend for Zn wt% and for Zn/C ratio showed behavior similar to height of ZnO measured via AFM, in that it increased as the dose rose from 0 to 300 pJ^2 s, then plateaued. Thus, we can conclude that the optimal irradiation parameters for smooth and continuous ZnO films deposition lay between 300 and 600 pJ^2 s at 200 °C.

In **Figure 4**, we demonstrate the suitability of our approach for depositing metal oxide over arbitrary template prepared with 2-PO on graphene. The AFM height images after two-photon oxidation and consequent ALD are presented in Figure 4a,b, respectively. The patterns prepared under various laser exposures had heights up to 2 nm (Figure 4c, for experimental conditions see Figure S5, Supporting Information), and the oxidation level and line width increased with increasing the laser exposure, as described previously. The presently achieved spatial resolution of ≈300 nm was limited by the optics in the current setup[25] but can be improved by tighter focusing of the laser beam. The ALD of ZnO carried out here for 63 cycles at 200 °C led to selective deposition of an up to 6-nm-thick layer of ZnO on the 2-PO-fabricated patterns (Figure 4c), depending on the oxidation level. The thin ZnO film deposition excellently preserved the original shape, position, and spatial resolution of the oxidized areas. The oxidized patterns guided the deposition

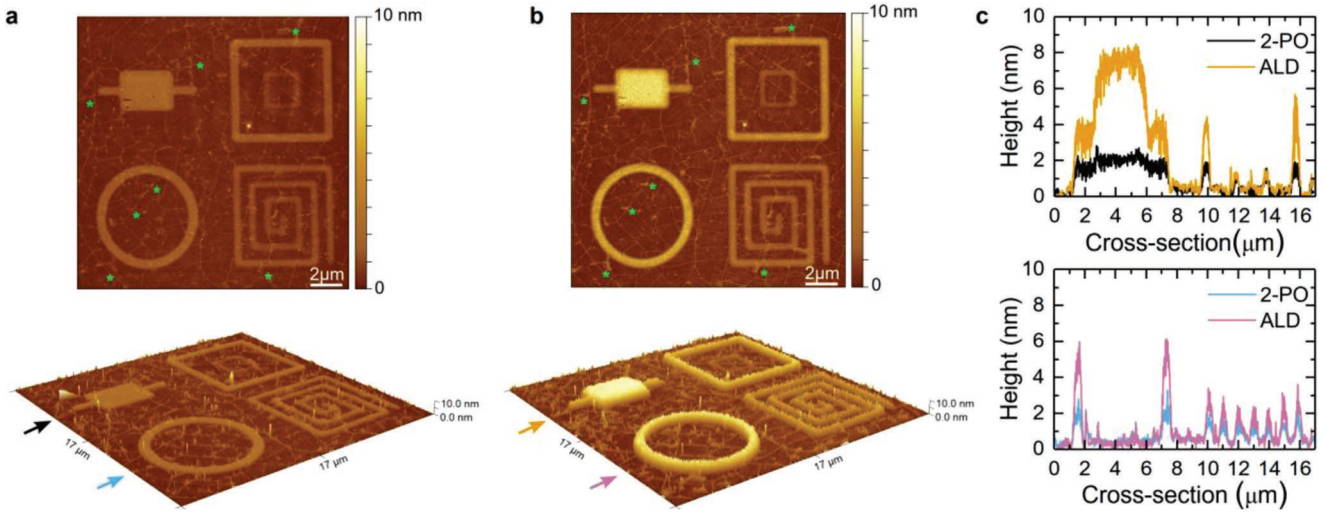

Figure 4. Area-selective atomic layer deposition on arbitrary patterned graphene. 2D and 3D AFM images of laser oxidized patterns: a) before and b) after 63 ALD cycles at 200 °C, and c) corresponding narrow cross-sections drawn through the middle of the patterns (see color-coded arrows). Green asterisks indicate few examples of the SiO_2 exposed due to rupture of graphene layer during AFM contact mode cleaning.

© 2022 The Authors. Advanced Materials Interfaces published by Wiley-VCH GmbH

with high precision, therefore, allowing to avoid a pattern placement error, which is a frequent problem in the fabrication of nanoscale devices. Minor deposition was observed on the graphene wrinkles and SiO_2 exposed during the rupture of graphene film during the contact mode cleaning. Our procedure can be beneficial in the miniaturization of electronic devices, where precise and selective preparation of well-defined patterns with nanoscale features is important. Near-field optics may be exploited to further reduce the spatial resolution. By focusing pulsed laser beam on an AFM tip, one should be able to generate a near field effect, which will allow for local graphene oxidation with a line width of ≈30 nm. The near field effect has already been demonstrated for 2D materials.[41–43]

Besides scaling down feature size, our approach has great potential for scaling-up sample fabrication. We demonstrated this with large 30×30 μm^2 patterns prepared with laser beam spot size of ≈25 μm (Figure S6, Supporting Information). The speed of the direct laser writing can be increased up to several cm per second for quick fabrication of enlarged active surface areas for ALD.

3. Conclusion

We demonstrated area-selective atomic layer deposition of ZnO on a laser-patterned graphene. ZnO was selectively deposited on the graphene areas that had been lightly to moderately oxidized by laser irradiation, while the growth on the pristine graphene surface was negligible. The densely packed functional groups created by the laser-induced two-photon oxidation procedure facilitated the precursor nucleation on the desired predefined areas. After the area-selective ALD process, oxidized graphene was converted back to pristine graphene by thermal annealing, without affecting the deposited ZnO film on the top of it, thus enabling tuning of the conductive properties of graphene. This shows that graphene is not only useful as a supporting growth layer for AS-ALD but can also be used as an active layer in device fabrication to increase the conductive properties of the system. The developed method has the potential for preparation of well-defined arbitrary patterns with feature sizes ranging from 300 nm up to centimeter scale. However, the lower resolution limit can be pushed down to ≈30 nm, by employing the near-field optics. Moreover, the procedure is suitable for the preparation of freestanding thin metal oxide films, where suspended graphene is used as growth-supporting layer and etched away after ALD. Finally, we envision the extension of our approach from the graphene-based devices to a wider variety of applications by using graphene as a transferable template for AS-ALD on other surfaces. As graphene can be transferred onto many other materials, this procedure may be appreciably versatile provided that the surface is compatible with the two-photon oxidation conditions.

4. Experimental Section

Sample Fabrication: The graphene was synthesized on Cu (111) thin films evaporated onto single-crystal sapphire (0001) substrates. The catalyst film was annealed at 1060 °C under gas flows of 470 sccm argon and 27 sccm hydrogen for 30 min to promote monocrystallinity through secondary grain growth. After annealing, the graphene growth was initiated by adding 6.8 sccm of 1% methane in argon to the furnace while keeping the temperature at 1060 °C. The growth time was 20 min. After the growth, the samples were taken out of the hot zone of the furnace and allowed to cool down. The graphene films were transferred by a standard PMMA transfer method[44] onto a target substrate, which was a silicon chip with a 300-nm thermal oxide film and a metal marker grid deposited on top. To transfer the graphene, a spin-coated PMMA layer acted as the graphene-support film and the copper was etched in 0.5 M ammonium persulfate solution leaving the graphene/PMMA stack floating on the liquid. Then, the graphene was rinsed in DI water, placed in 12% HCl to remove possible metal residues, rinsed again in DI water, and placed onto the Si/SiO_2 substrate. The PMMA film was removed with trichloroethylene (60 min at 40 °C). Finally, the sample was annealed at 300 °C in Ar/H_2 atmosphere for 2 h to remove PMMA residues.

Two-Photon Oxidation: Two-photon oxidation of graphene was performed with 515 nm femtosecond laser (Pharos-10, Light Conversion Ltd., 600 kHz repetition rate, 250 fs pulse duration) in ambient atmosphere at a relative humidity of 35%. Experiments were performed in two configurations:

– *Small beam oxidation*. The femtosecond laser was focused with an objective lens (N.A. = 0.8) to a single Gaussian spot (a diameter at $1/e^2$ of ≈1.2 μm). Graphene was irradiated using a range of laser pulse energies (10–25 pJ) and an exposure time of up to 1 s per spot, to produce patterns with different oxidation levels. The matrices of squares with sizes of $\approx 2 \times 2$ μm^2 were patterned by step-by-step irradiation, with 0.1 μm separation between consecutive laser spots.

– *Large beam oxidation*. To oxidize large areas, 2x objective was used with a spot diameter of ≈25 μm. The pulse energies ranged from 1 to 6.5 nJ and the time was from 0.1 to 1.5 s per spot. We made 30×30 μm^2 2-PO patterns with 4 μm separation between each two spots.

Atomic Layer Deposition: For the ALD deposition of ZnO using DEZ and water, a commercial flow-type hot-wall ALD reactor (F-120 by ASM Ltd) was used. Both DEZ precursor ($Zn(CH_2CH_3)_2$; Sigma-Aldrich, ≥ 52 wt% Zn basis) and the deionized water cylinders were kept outside the reactor at room temperature. Nitrogen (N_2, 99.999%, flow rate at 300 SCCM) was used as both the precursor carrier gas and the purge gas between the precursor pulses. The reactor pressure was kept between 3 and 5 mbar. The ZnO films were deposited at 150, 200, and 250 °C on both graphene and on Si (100) substrates with a native oxide layer, the latter was used for the thickness determination. The precursor pulse lengths were based on our previous studies using same precursors and the reactor.[45] Since the deposition temperature was lower in comparison, long purges were applied in order to make sure that there was only one precursor in the reactor at a time. The following pulse/purge lengths were used; 1 s DEZ/4 s N_2/1.5 s H_2O/6 s N_2. The total number of ALD cycles was chosen according to the target thickness.

X-Ray Reflection: The thicknesses of ZnO films grown on silicon were determined with X-ray reflection (XRR; Panalytical XPert diffractometer, Cu Kα source) followed by fitting the data with X'Pert Reflectivity software by PANalytical.

Atomic Force Microscopy: Cleaning residuals from the samples after transfer was accomplished using contact mode on a Bruker Dimension Icon atomic force microscope. Soft NSG03 cantilevers with force constant less than 1 N m^{-1} from NT-MDT were used to minimize the defect introduction during the cleaning. AFM imaging was carried out on a Bruker Dimension Icon atomic force microscope using Peak Force Tapping mode. ScanAsyst-Air probes from Bruker were used during imaging with the peak force set to 2.0 nN. All AFM images were processed with Gwyddion software.

Raman Spectroscopy: A DXR Raman (Thermo Scientific) with a 50x objective was used for mapping and spectra acquisition. The laser power was 1 mW and 532 nm of excitation was utilized.

Energy-Dispersive X-Ray Spectroscopy (EDS): A Zeiss EVO-50XVP scanning electron microscope was used in combination with a Bruker

© 2022 The Authors. Advanced Materials Interfaces published by Wiley-VCH GmbH

Quantax 400 EDS system. The electron high tension was kept at 5 kV. The time per point in single-point experiments was 1 min and 15 s per point during the mapping.

Supporting Information

Supporting Information is available from the Wiley Online Library or from the author.

Acknowledgements

The authors acknowledge fundings from the Academy of Finland (Flagship PREIN and grant no. 311330), and from the Jane and Aatos Erkko Foundation. The authors like to acknowledge the use of the RawMatters Finland Infrastructure (RAMI) at Aalto University. The authors acknowledge Olli Rissanen for synthetizing the graphene samples and Erich See for proofreading the manuscript.

Conflict of Interest

The authors declare no conflict of interest.

Data Availability Statement

The data that support the findings of this study are available from the corresponding author upon reasonable request.

Keywords

atomic layer deposition, graphene, surface engineering, two-photon oxidation

Received: May 19, 2022
Revised: July 9, 2022
Published online:

[1] M. Knez, K. Nielsch, L. Niinistö, *Adv. Mater.* **2007**, *19*, 3425.
[2] R. Chen, S. F. Bent, *Adv. Mater.* **2006**, *18*, 1086.
[3] A. J. M. Mackus, A. A. Bol, W. M. M. Kessels, *Nanoscale* **2014**, *6*, 10941.
[4] A. J. M. Mackus, M. J. M. Merkx, W. M. M. Kessels, *Chem. Mater.* **2019**, *31*, 2.
[5] G. N. Parsons, R. D. Clark, *Chem. Mater.* **2020**, *32*, 4920.
[6] R. H. A. Ras, E. Sahramo, J. Malm, J. Raula, M. Karppinen, *J. Am. Chem. Soc.* **2008**, *130*, 11252.
[7] A. J. M. Mackus, S. A. F. Dielissen, J. J. L. Mulders, W. M. M. Kessels, *Nanoscale* **2012**, *4*, 4477.
[8] W.-H. Kim, K. Shin, B. Shong, L. Godet, S. F. Bent, *Chem. Mater.* **2020**, *32*, 9696.
[9] S. Balasubramanyam, M. J. M. Merkx, M. A. Verheijen, W. M. M. Kessels, A. J. M. Mackus, A. A. Bol, *ACS Mater. Lett.* **2020**, *2*, 511.
[10] M. Krishtab, S. Armini, J. Meersschaut, S. de Gendt, R. Ameloot, *ACS Appl. Mater. Interfaces* **2021**, *13*, 32381.
[11] I.-K. Oh, T. E. Sandoval, T.-L. Liu, N. E. Richey, S. F. Bent, *Chem. Mater.* **2021**, *33*, 3926.
[12] J. Lu, J. W. Elam, P. C. Stair, *Surf. Sci. Rep.* **2016**, *71*, 410.
[13] B. D. Boruah, *Nanoscale Adv.* **2019**, *1*, 2059.
[14] E. Comini, *Mater. Today* **2016**, *19*, 559.
[15] S. Kasap, I. I. Kaya, S. Repp, E. Erdem, *Nanoscale Adv.* **2019**, *1*, 2586.
[16] B. Xue, Y. Zou, *J. Colloid Interface Sci.* **2018**, *529*, 306.
[17] N. O. Weiss, H. Zhou, L. Liao, Y. Liu, S. Jiang, Y. Huang, X. Duan, *Adv. Mater.* **2012**, *24*, 5782.
[18] A. C. Ferrari, F. Bonaccorso, V. Falko, K. S. Novoselov, S. Roche, P. Bøggild, S. Borini, F. H. L. Koppens, V. Palermo, N. Pugno, J. A. Garrido, R. Sordan, A. Bianco, L. Ballerini, M. Prato, E. Lidorikis, J. Kivioja, C. Marinelli, T. Ryhänen, A. Morpurgo, J. N. Coleman, V. Nicolosi, L. Colombo, A. Fert, M. Garcia-Hernandez, A. Bachtold, G. F. Schneider, F. Guinea, C. Dekker, M. Barbone, et al., *Nanoscale* **2015**, *7*, 4598.
[19] V. Wheeler, N. Garces, L. Nyakiti, R. Myers-Ward, G. Jernigan, J. Culbertson, C. Eddy, D. K. Gaskill, *Carbon N Y* **2012**, *50*, 2307.
[20] X. Wang, S. Tabakman, H. Dai, *J. Am. Chem. Soc.* **2008**, *130*, 8152.
[21] J. M. P. Alaboson, C.-H. Sham, S. Kewalramani, J. D. Emery, J. E. Johns, A. Deshpande, T. Chien, M. J. Bedzyk, J. W. Elam, M. J. Pellin, M. C. Hersam, *Nano Lett.* **2013**, *13*, 5763.
[22] R. H. J. Vervuurt, B. Karasulu, M. A. Verheijen, W. (Erwin), M. M. Kessels, A. A. Bol, *Chem. Mater.* **2017**, *29*, 2090.
[23] J. I. Paez-Ornelas, H. N. Fernández-Escamilla, H. A. Borbón-Nuñez, H. Tiznado, N. Takeuchi, J. Guerrero-Sánchez, *Phys. Chem. Chem. Phys.* **2021**, *23*, 3467.
[24] W. Ke, Y. Liu, X. Wang, X. Qin, L. Chen, R. M. Palomino, J. P. Simonovis, I. Lee, I. Waluyo, J. A. Rodriguez, A. I. Frenkel, P. Liu, F. Zaera, *Nano Lett.* **2020**, *20*, 6884.
[25] J. Aumanen, A. Johansson, J. Koivistoinen, P. Myllyperkiö, M. Pettersson, *Nanoscale* **2015**, *7*, 2851.
[26] J. Koivistoinen, L. Sládková, J. Aumanen, P. Koskinen, K. Roberts, A. Johansson, P. Myllyperkiö, M. Pettersson, *J. Phys. Chem. C* **2016**, *120*, 22330.
[27] M. E. Mendoza, E. H. M. Ferreira, A. Kuznetsov, C. A. Achete, J. Aumanen, P. Myllyperkiö, A. Johansson, M. Pettersson, B. S. Archanjo, *Carbon N Y* **2019**, *143*, 720.
[28] A. Johansson, H.-C. Tsai, J. Aumanen, J. Koivistoinen, P. Myllyperkiö, Y.-Z. Hung, M.-C. Chuang, C.-H. Chen, W. Y. Woon, M. Pettersson, *Carbon N Y* **2017**, *115*, 77.
[29] T. Tynell, M. Karppinen, *Semicond. Sci. Technol.* **2014**, *29*, 043001.
[30] A. V. Emelianov, D. Kireev, A. Offenhäusser, N. Otero, P. M. Romero, I. I. Bobrinetskiy, *ACS Photonics* **2018**, *5*, 3107.
[31] R. H. J. Vervuurt, W. M. M. E. Kessels, A. A. Bol, *Adv. Mater. Interfaces* **2017**, *4*, 1700232.
[32] Y.-C. Lin, C.-C. Lu, C.-H. Yeh, C. Jin, K. Suenaga, P.-W. Chiu, *Nano Lett.* **2012**, *12*, 414.
[33] J. Malm, E. Sahramo, J. Perälä, T. Sajavaara, M. Karppinen, *Thin Solid Films* **2011**, *519*, 5319.
[34] M. A. Gomez-Alvarez, C. Morales, J. Méndez, A. del Campo, F. J. Urbanos, A. Díaz, L. Reséndiz, J. I. Flege, D. Granados, L. Soriano, *C — Journal of Carbon Research* **2020**, *6*, 41.
[35] A. C. Ferrari, *Solid State Commun.* **2007**, *143*, 47.
[36] L. Gustavo Cançado, M. Gomes da Silva, E. H. Martins Ferreira, F. Hof, K. Kampioti, K. Huang, A. Pénicaud, C. Alberto Achete, R. B. Capaz, A. Jorio, *2D Mater.* **2017**, *4*, 025039.
[37] Z. H. Ni, H. M. Wang, Y. Ma, J. Kasim, Y. H. Wu, Z. X. Shen, *ACS Nano* **2008**, *2*, 1033.
[38] D. W. Li, Q. M. Zou, X. Huang, H. Rabiee Golgir, K. Keramatnejad, J. F. Song, Z. Y. Xiao, L. S. Fan, X. Hong, L. Jiang, J. F. Silvain, S. Sun, Y. F. Lu, *Nanoscale* **2017**, *9*, 8997.
[39] E. Zion, A. Butenko, Y. Kaganovskii, V. Richter, L. Wolfson, A. Sharoni, E. Kogan, M. Kaveh, I. Shlimak, *J. Appl. Phys.* **2017**, *121*, 114301.

© 2022 The Authors. Advanced Materials Interfaces published by Wiley-VCH GmbH

[40] R. Liu, M. Peng, H. Zhang, X. Wan, M. Shen, *Mater. Sci. Semicond. Process.* **2016**, *56*, 324.
[41] Z. Fei, A. S. Rodin, G. O. Andreev, W. Bao, A. S. McLeod, M. Wagner, L. M. Zhang, Z. Zhao, M. Thiemens, G. Dominguez, M. M. Fogler, A. H. C. Neto, C. N. Lau, F. Keilmann, D. N. Basov, *Nature* **2012**, *487*, 82.
[42] Y. Kim, J. Kim, *Nanophotonics* **2021**, *10*, 3397.
[43] B. Lyu, H. Li, L. Jiang, W. Shan, C. Hu, A. Deng, Z. Ying, L. Wang, Y. Zhang, H. A. Bechtel, M. C. Martin, T. Taniguchi, K. Watanabe, W. Luo, F. Wang, Z. Shi, *Nano Lett.* **2019**, *19*, 1982.
[44] J. W. Suk, A. Kitt, C. W. Magnuson, Y. Hao, S. Ahmed, J. An, A. K. Swan, B. B. Goldberg, R. S. Ruoff, *ACS Nano* **2011**, *5*, 6916.
[45] R. Ghiyasi, G. C. Tewari, M. Karppinen, *J. Phys. Chem. C* **2020**, *124*, 13765.

© 2022 The Authors. Advanced Materials Interfaces published by Wiley-VCH GmbH